Processing-microstructure-property relationships

Contents

- ❑ Introduction
- ❑ General microstructural characteristics
- ❑ Restoration mechanisms
- ❑ Modelling approaches
- ❑ Summary

Introduction

- Grain size control
- Microsegregation
- Precipitation
- Texture
- Twinning
- Deformation-induced transformations

- Strength and ductility
- Toughness
- Fatigue
- Corrosion
- Irradiation resistance

General microstructural characteristics

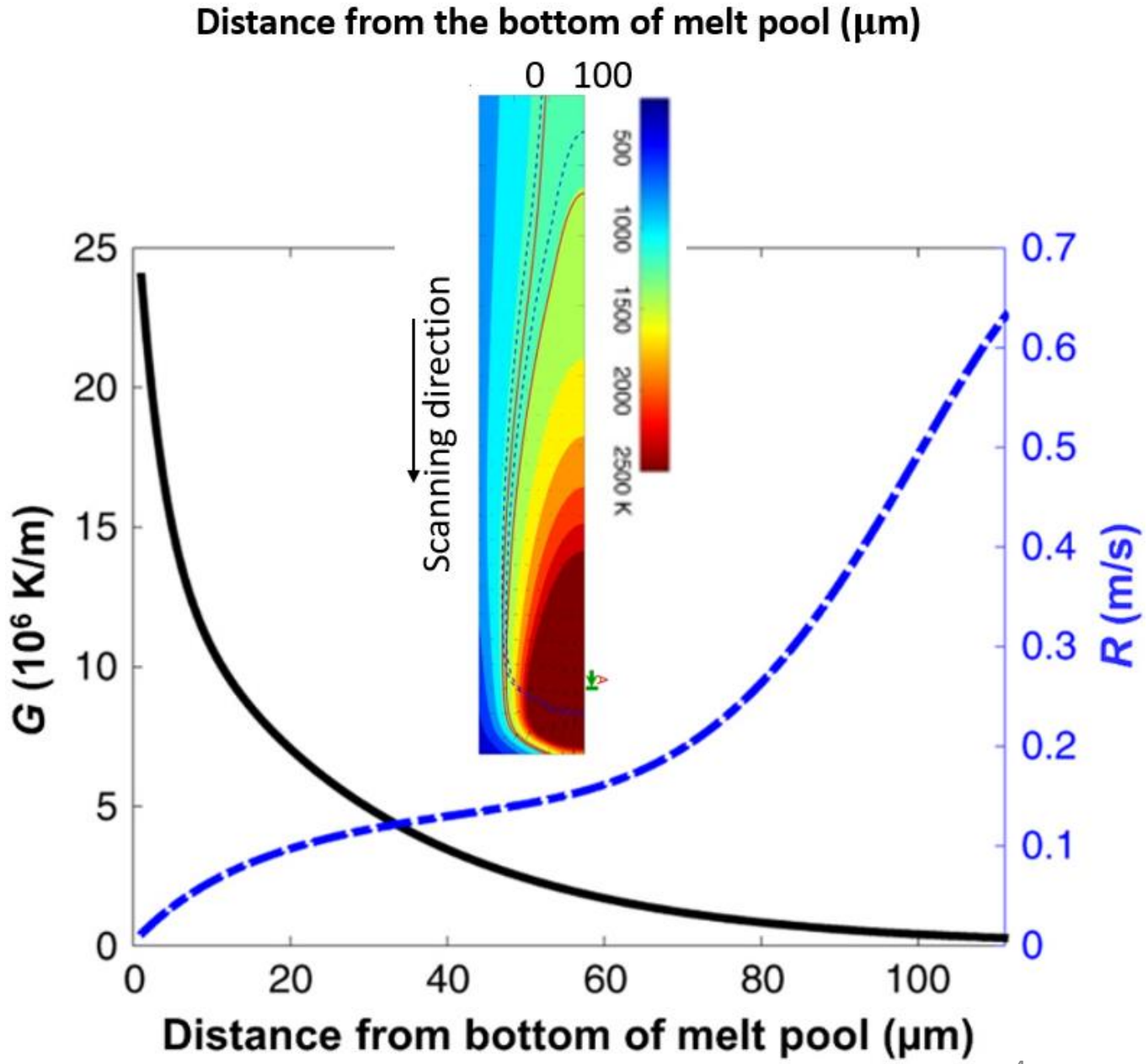

Fig. Thermal gradient (G) variation with distance form the bottom of the melt pool
(R: solidification speed, G:Thermal gradient)

Source: Pham et al. 2020 [https://doi.org/10.1038/s41467-020-14453-3]

General microstructural characteristics

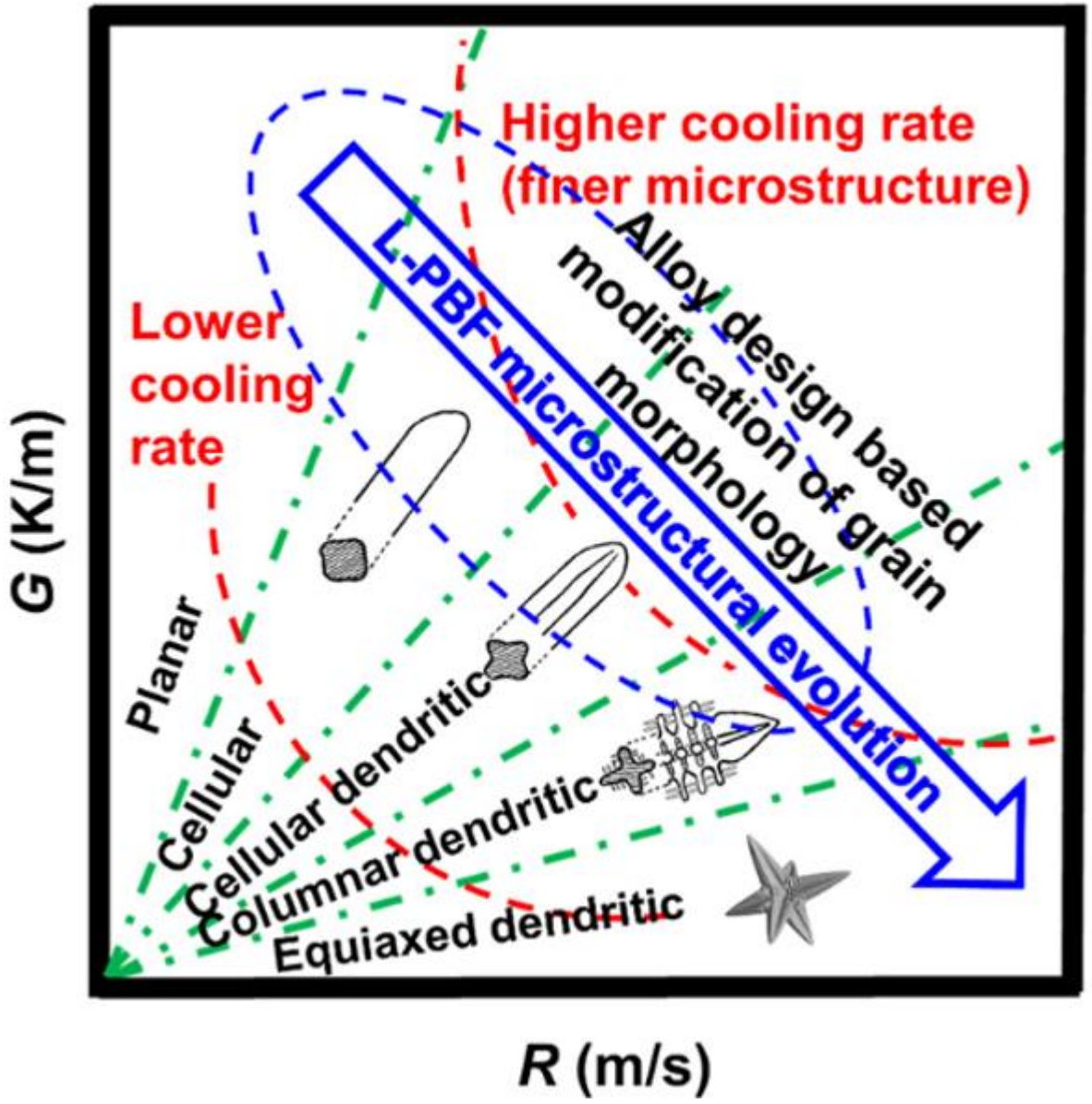

Fig. Expected microstructures resulting from (R: solidification speed, G:Thermal gradient)

Mishra and Thapliyal 2021 [https://doi.org/10.1016/j.matdes.2021.109640]

General microstructural characteristics

Fig. Typical variation in temperature for Subsequent printed layers L1, L2, …

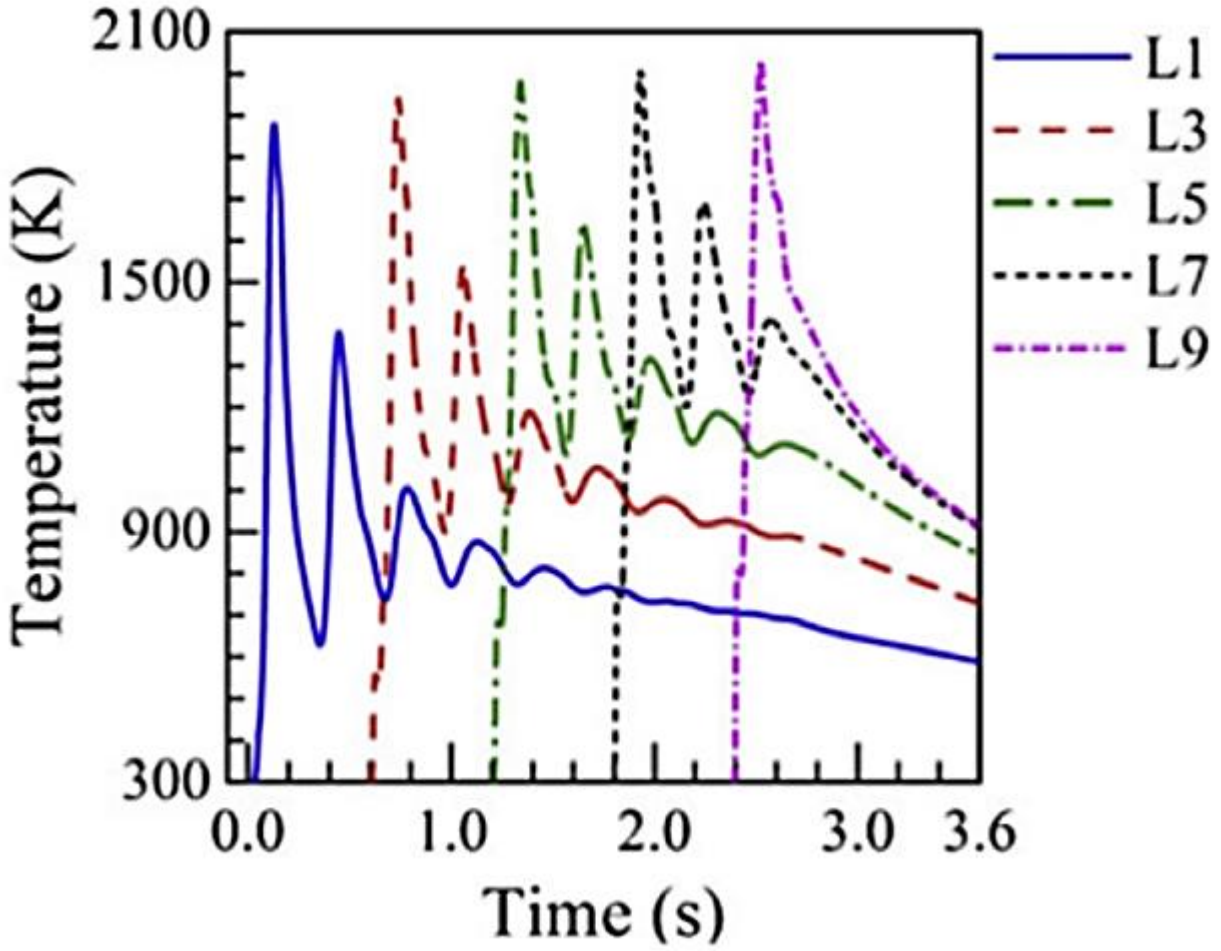

Source: Kirka et al. 2017 [http://dx.doi.org/10.1016/j.scriptamat.2017.01.005]

General microstructural characteristics

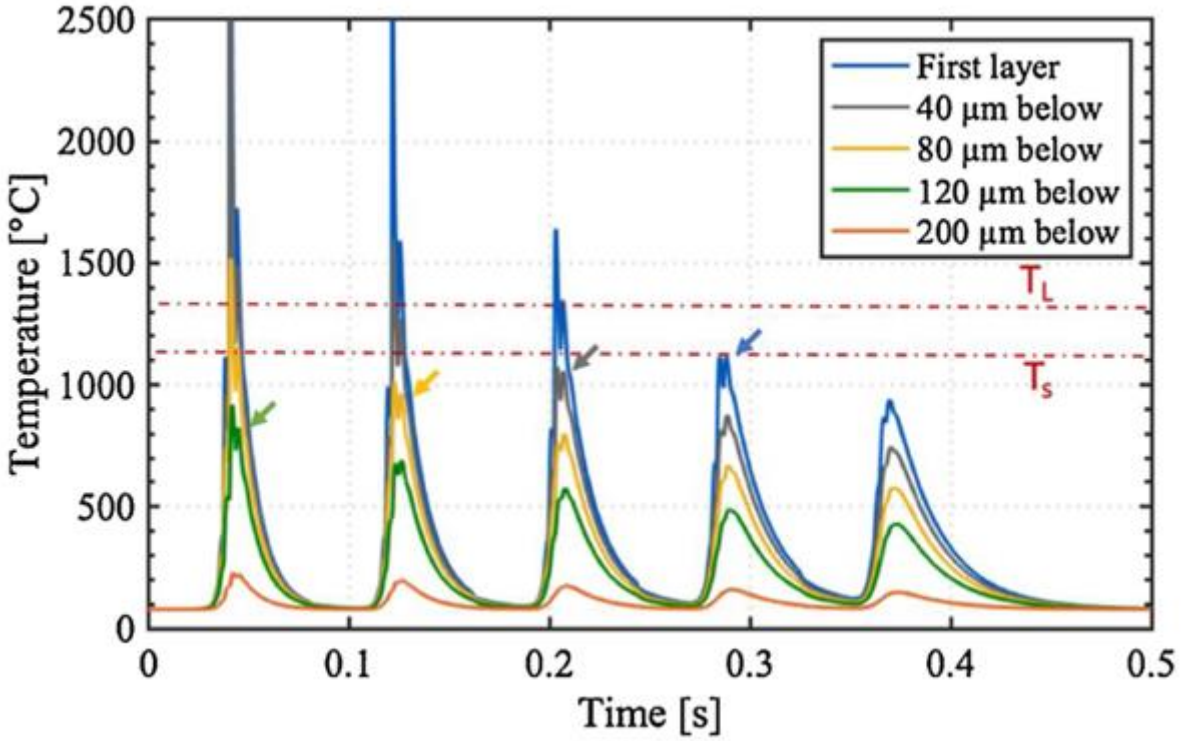

Fig. Typical temperature variation at a given point in the subsurface

Note: the time axis is shifted as the laser is approximately approaching the reference point

Source: Jiang et al. 2020 [https://doi.org/10.1016/j.addma.2020.101282]

General microstructural characteristics

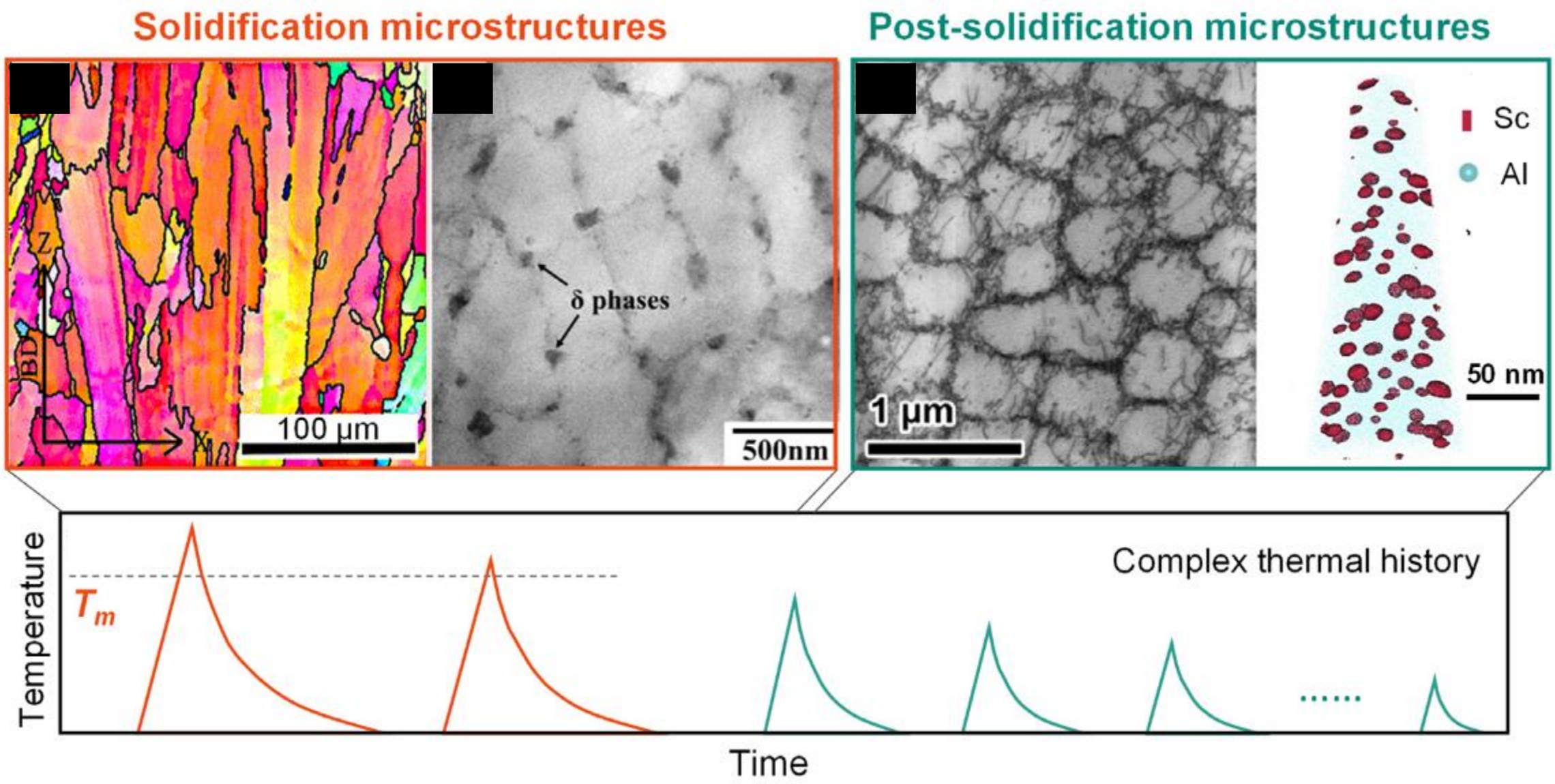

Source: Liu et al . 2022 [https://doi.org/10.1016/j.jmst.2021.06.011]

General microstructural characteristics

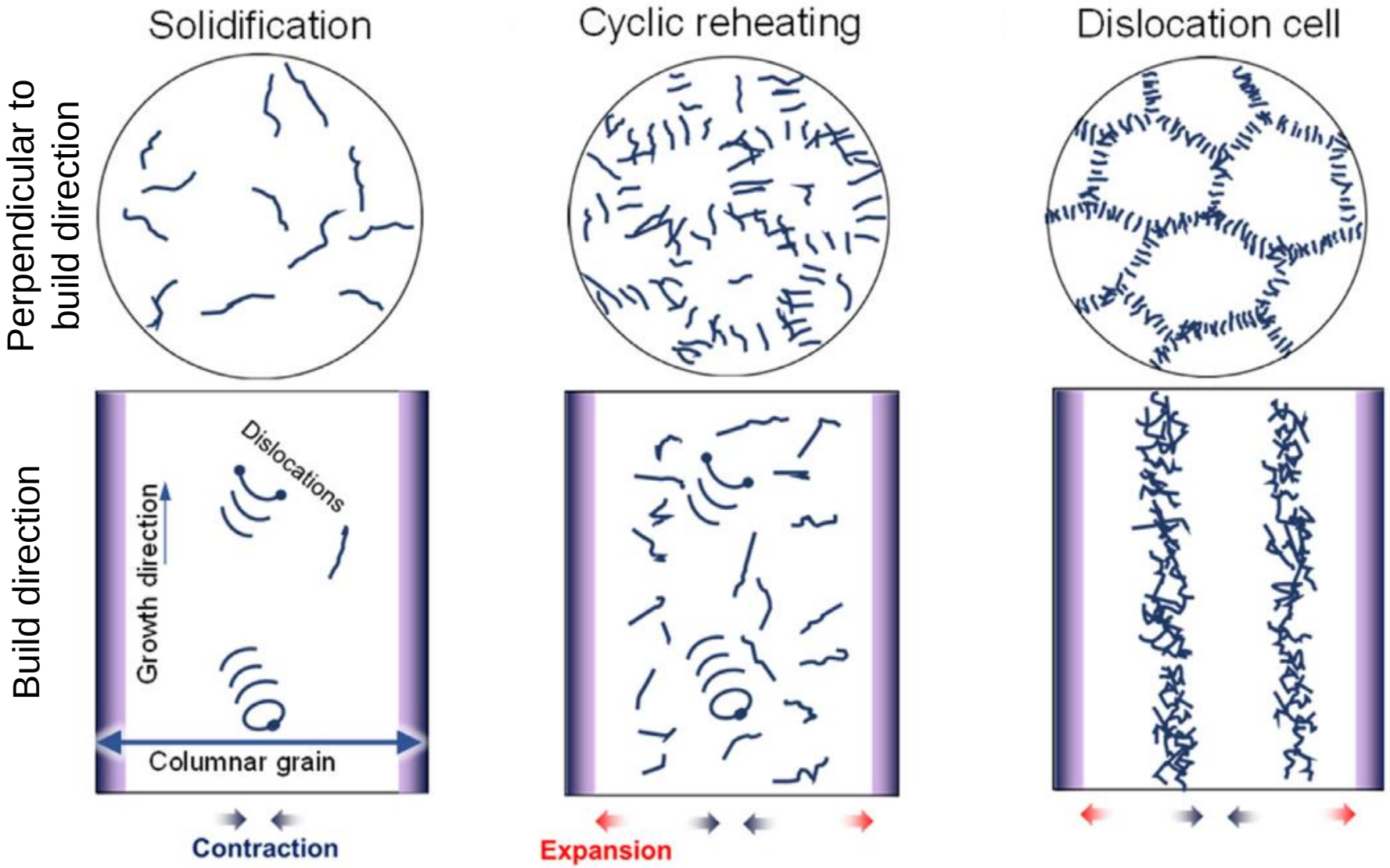

Fig. Schematics of dislocation cell formation during AM thermal cycling

Source: Liu et al . 2022 [https://doi.org/10.1016/j.jmst.2021.06.011]

Restoration mechanisms

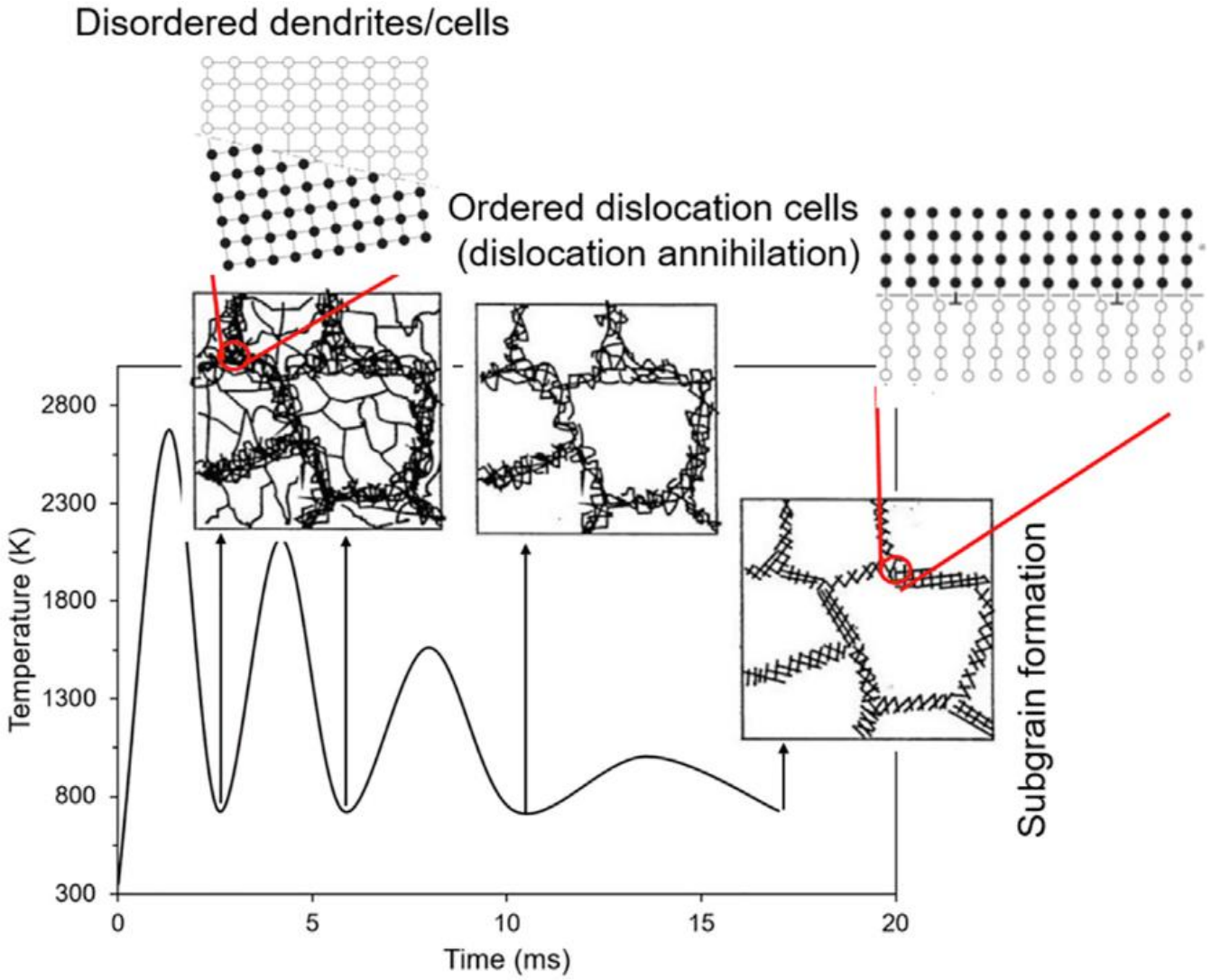

Fig. Typical dislocation cell structures formed at various stages of heating and cooling

Source: Sabzi et al. 2021 [https://doi.org/10.1016/j.matdes.2021.110246]

Restoration mechanisms

Fig. Variation of recovery, continuous (CDRX) And discontinuous dynamic recrystallization (DDRX) at various strain stages and for various Strain rates

Where,

$\dot{\varepsilon}$: strain rate

$\dot{\varepsilon}_c^T$: critical strain rate for Dynamic recrystallization activation

$\varepsilon_c^{c/T}$: critical strain for the Formation of high-angle grain boundaries

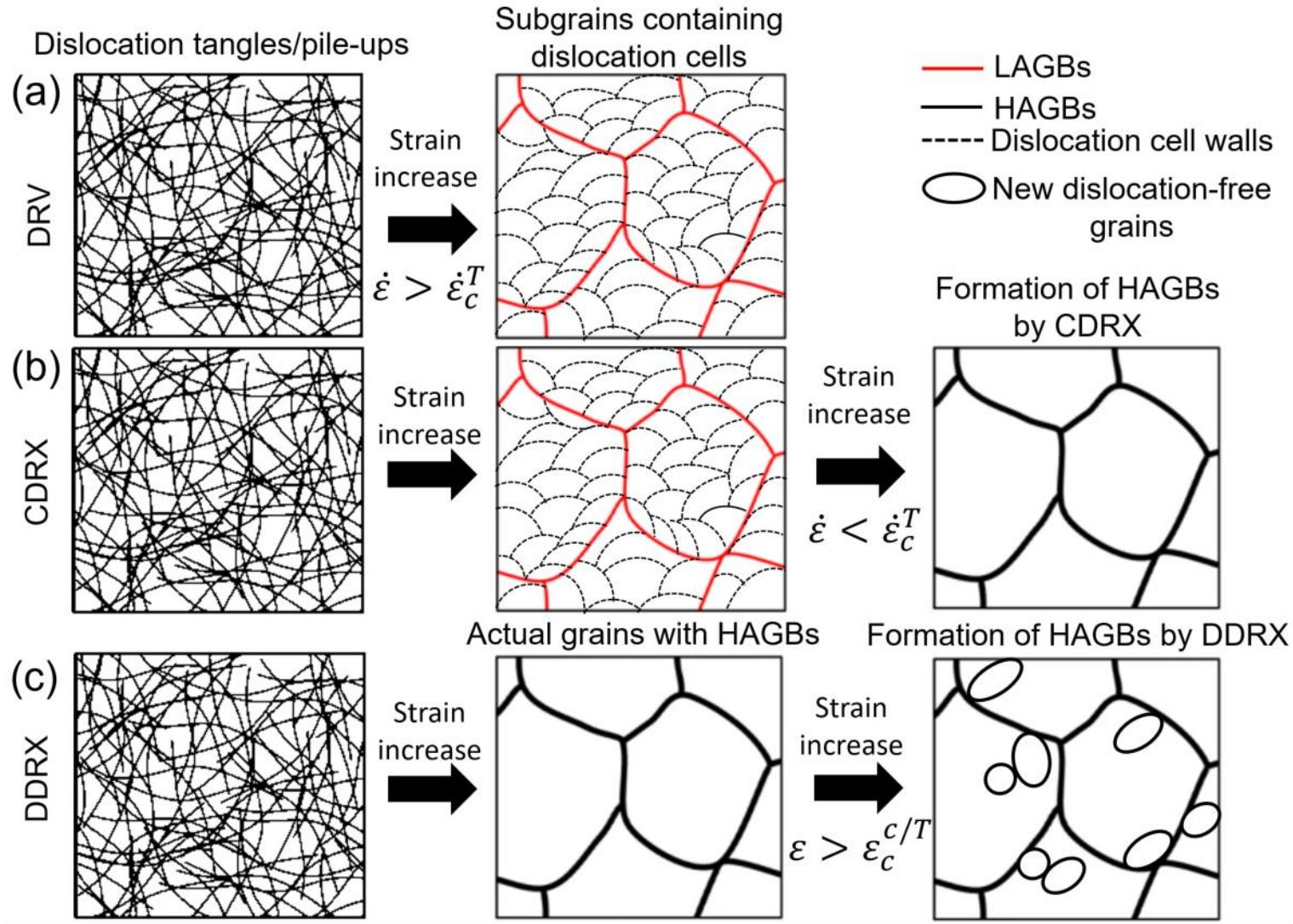

Source: Sabzi et al. 2021 [https://doi.org/10.1016/j.matdes.2021.110246]

Restoration mechanisms

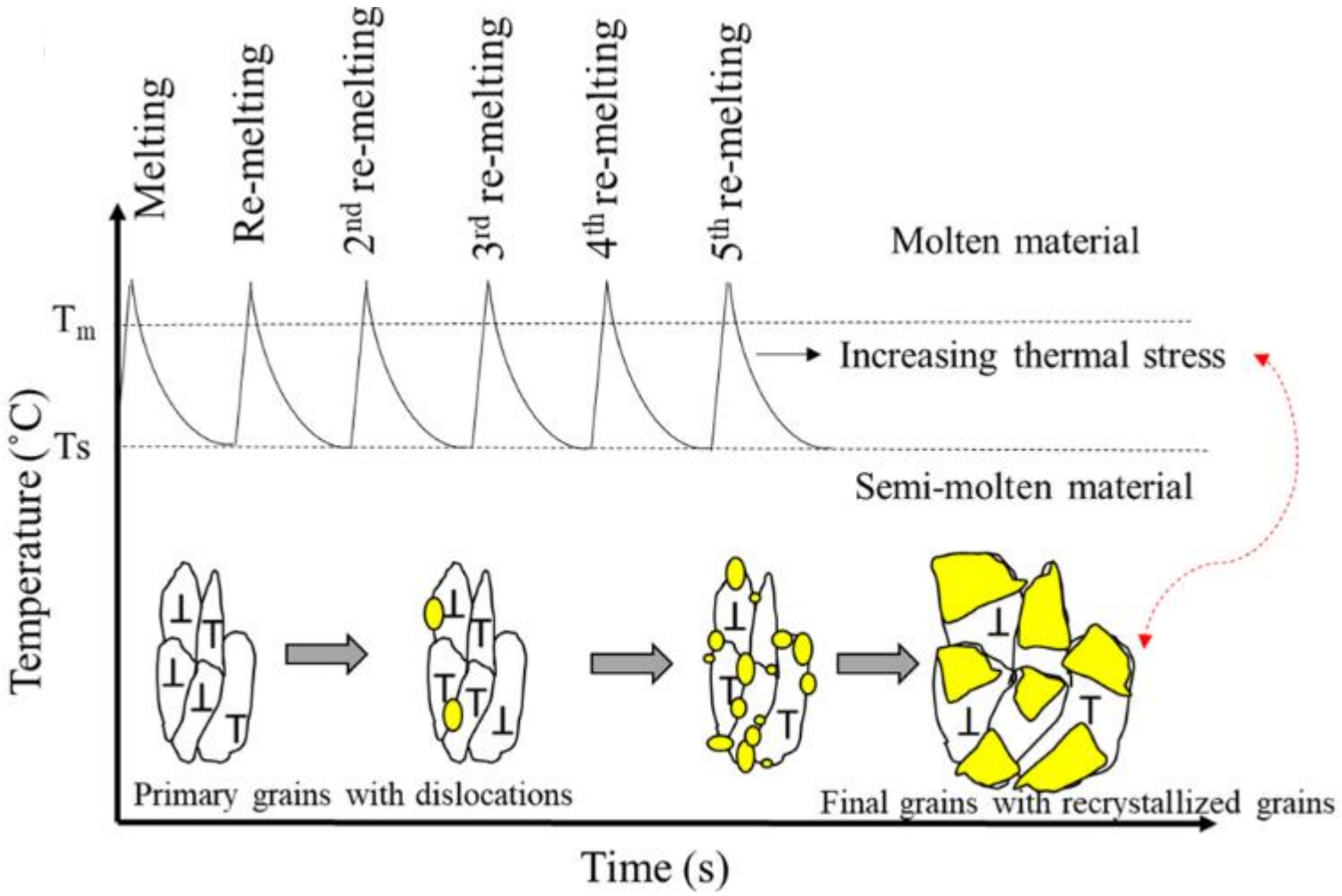

Fig. Remelting stages influence on substructure formation

Source: Karimi et al. 2021 [https://doi.org/10.1016/j.addma.2021.102086]

Restoration mechanisms

Fig. Influence of build direction on Microstructural orientation (a) Sample SS-0, (b) sample SS-90, and (c) sample SS-67, and (d) volume fraction of recrystallization.

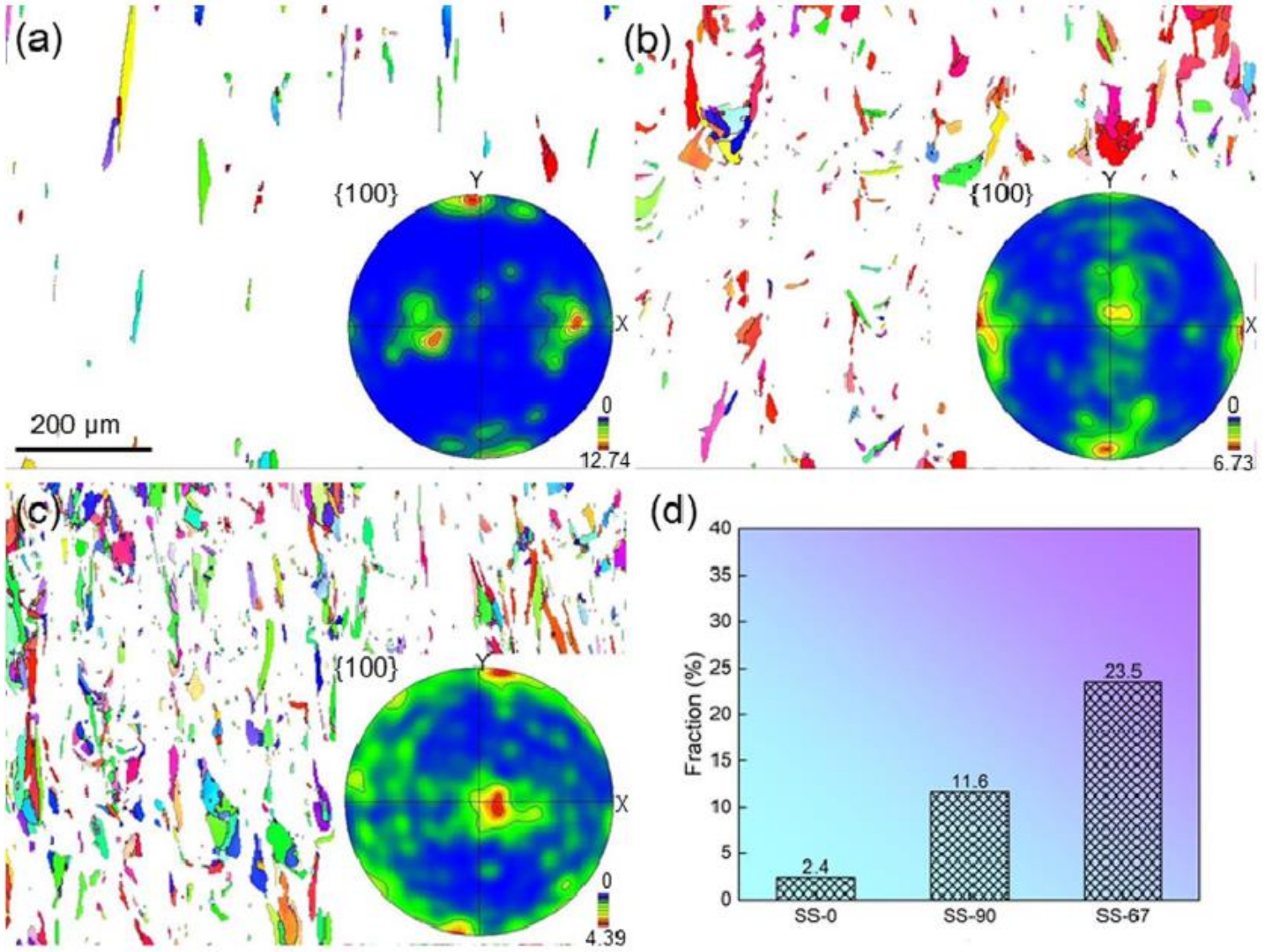

Source: Xu et al. 2021 [https://doi.org/10.1016/j.matdes.2021.109940]

Modelling approaches

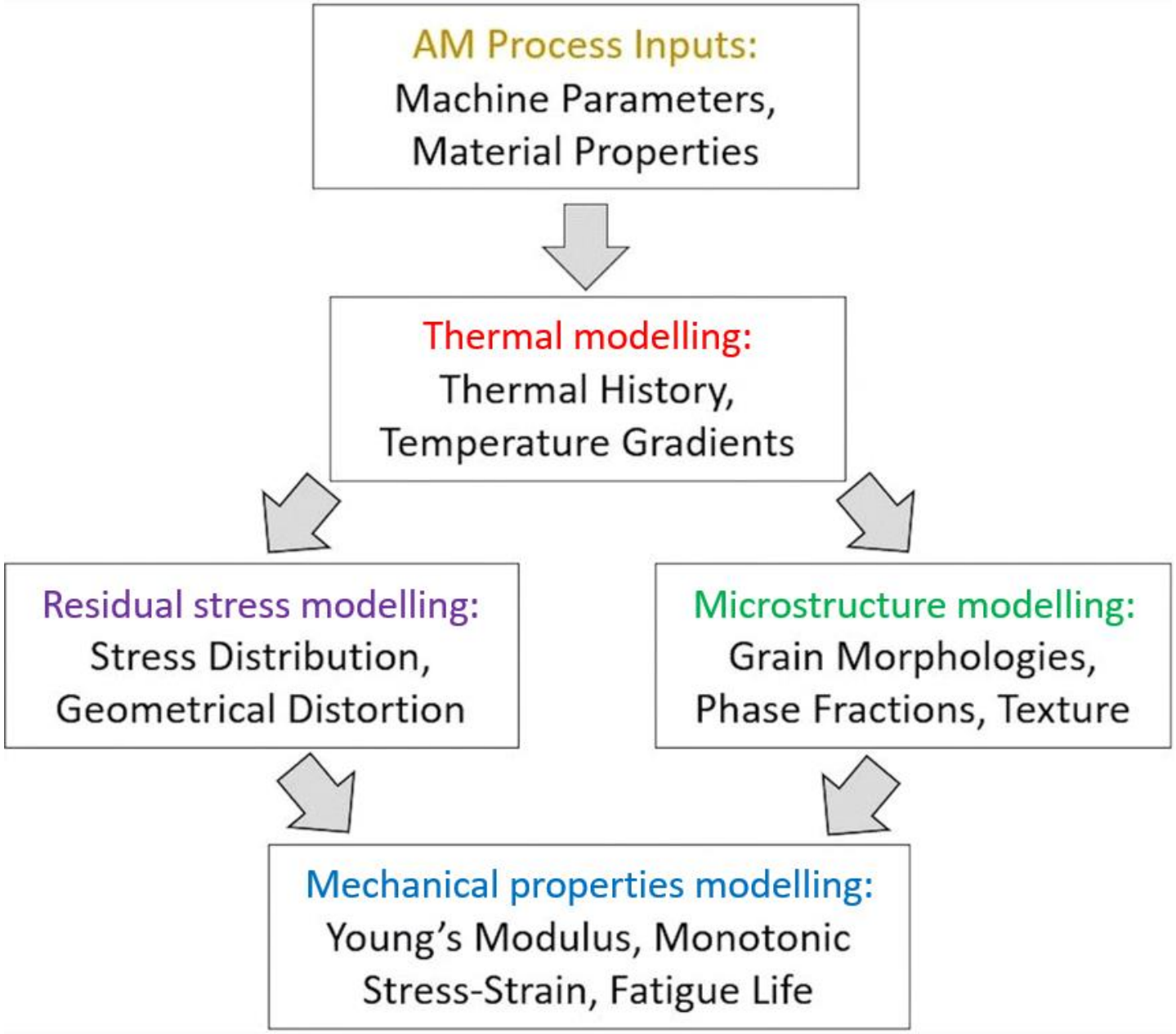

Fig. Workflow of AM modelling

Source: Gatsos et al. 2020 [https://doi.org/10.1007/s11837-019-03913-x]

Modelling approaches

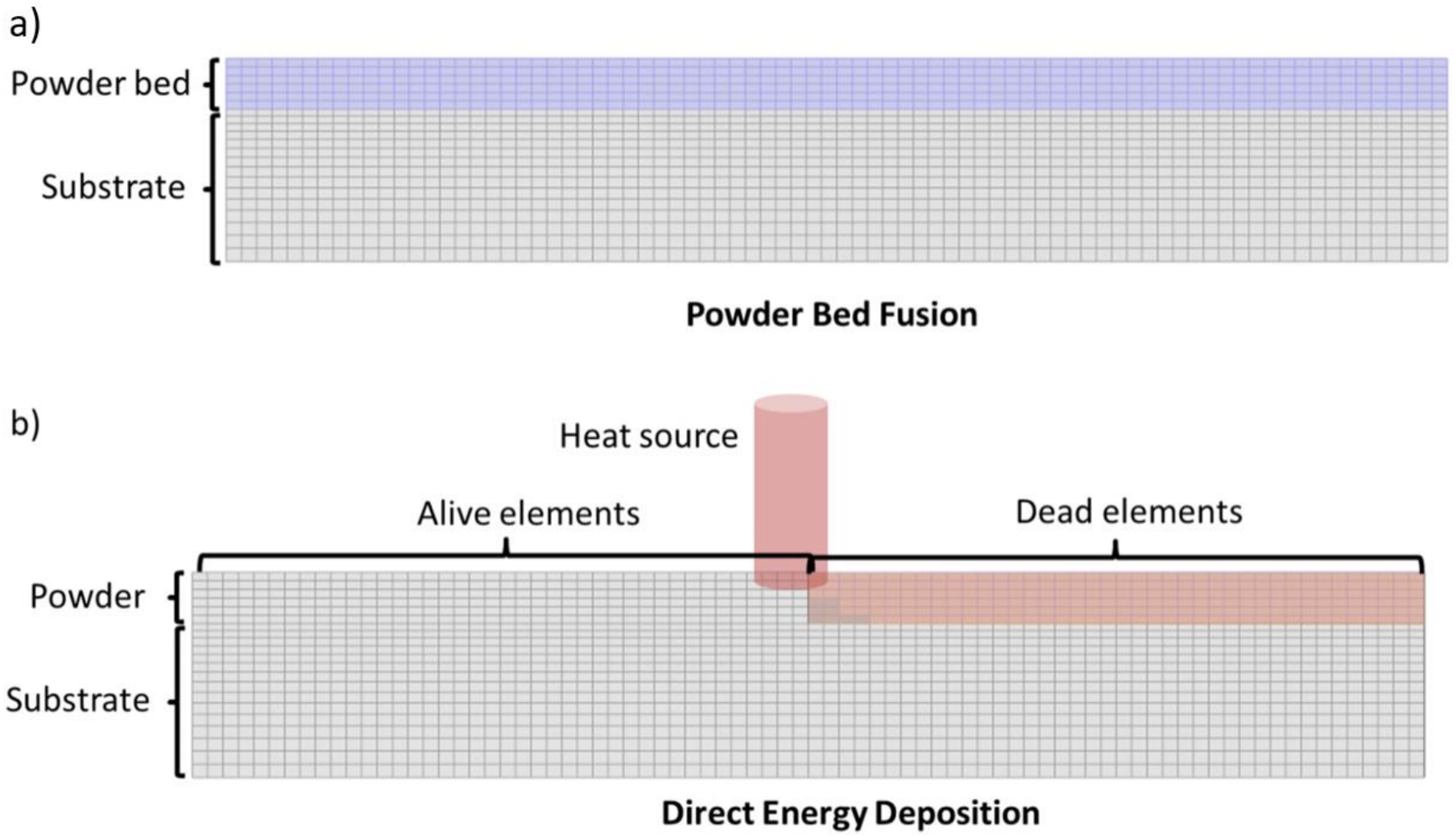

Fig. Description of element configurations in meting stages

Source: Tan et al. 2020 [https://doi.org/10.1080/17452759.2019.1677345]

Residual stress and distortion equations

$$\nabla \cdot \sigma = 0$$

$$\sigma = C\epsilon$$

$$\epsilon = \epsilon_e + \epsilon_p + \epsilon_T + \epsilon_V$$

$$\epsilon_T = \alpha_{CTE}(T - T_{ref})$$

σ: residual stress
ϵ: distortion
C: stiffness tensor

ϵ_e: elastic strain
ϵ_p: plastic strain
ϵ_T: thermal strain
ϵ_V thermal strain due to phase transformations

α_{CTE} :coefficient of thermal expansion
T_{ref} : is the reference temperature

Modelling approaches

Microstructure Models

Phase Field Method

Boundary conditions:

- Initial temperature
- Temperature gradient
- Melt pool angle
- Fluid flow
- Nucleation density
- Seeded dendrite angles

Assumptions:

- Growth from seeded round dendrites
- Material reduced to binary alloy

Kinetic Monte Carlo

Boundary conditions:

- Melt pool temperature
- Melt pool shape

Assumptions:

- Lowest energy state of each time step is the resultant microstructure

Cellular Automata

Boundary conditions:

- Melt pool temperature
- Melt pool shape
- Nucleation density
- Seeded grain angles

Assumptions:

- Solidification theory holds for given thermal profile
- Dendrites grow in the <100> direction

Source: Tan et al. 2020 [https://doi.org/10.1080/17452759.2019.1677345]

Modelling approaches – Phase field simulations of orientation

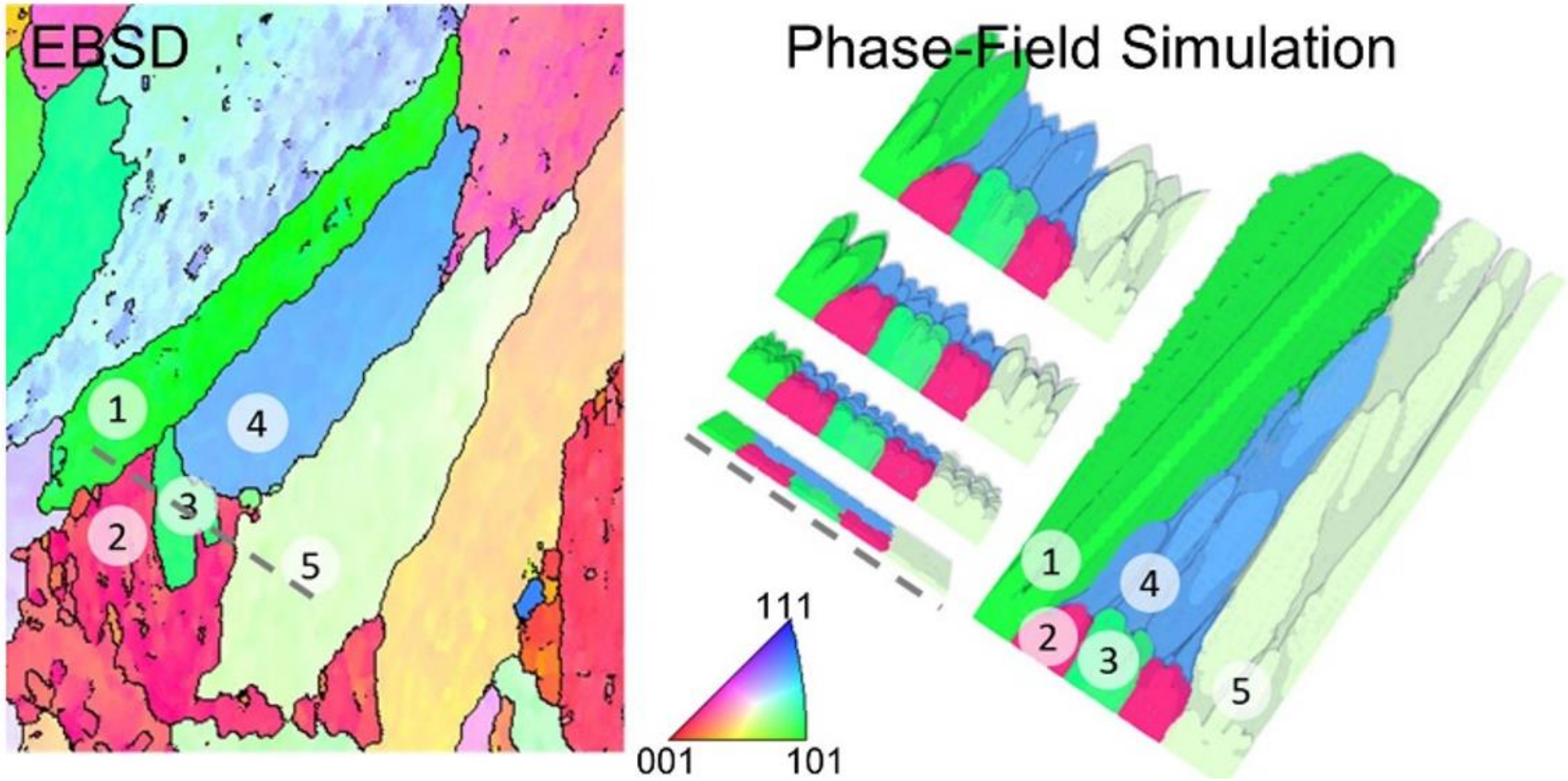

Fig. Accuracy of Phase field simulation for grain morphology and orientation

Source: Park et al. 2020 [https://doi.org/10.1016/j.matdes.2020.108985]

Phase field modelling equations

$$\frac{\partial \phi}{\partial t} = L \frac{\partial F}{\partial \phi}$$

$$F = \int \left[f_0(\phi, T) + \frac{1}{2} \kappa_\phi (\boldsymbol{\nabla} \phi)^2 \right] dV$$

$$f_0 = h f^S + (1 - h) f^L + Q f$$

$$\kappa_\phi = \frac{9 \gamma^2}{32 \Delta f}$$

F: microstructure free energy functional
L: kinetic rate coefficient

$f_0(\varphi, T)$:local free energy density,
V: volume,
κ_φ : gradient energy coefficient.

f^S and f^L : free energies of the solid and liquid phases, respectively,
Q: height of the activation barrier at the interface,
$h = \varphi^2(3-2\varphi)$, and
$f = \varphi^2 (1-\varphi)^2$

γ: specific interfacial energy (interfacial energy per unit area)

Monte Carlo mathematical formulation

$$P = \exp\left(-\frac{\Delta E}{k_B T_s}\right), \qquad \text{if} \quad \Delta \mathrm{E} > 0$$

$$P = 1, \qquad \text{if} \quad \Delta \mathrm{E} \leq 0$$

P: acceptance probability

k_B: Boltzmann constant,

$k_B T_s$: thermal fluctuation during simulation,

ΔE: overall system energy change

Modelling approaches

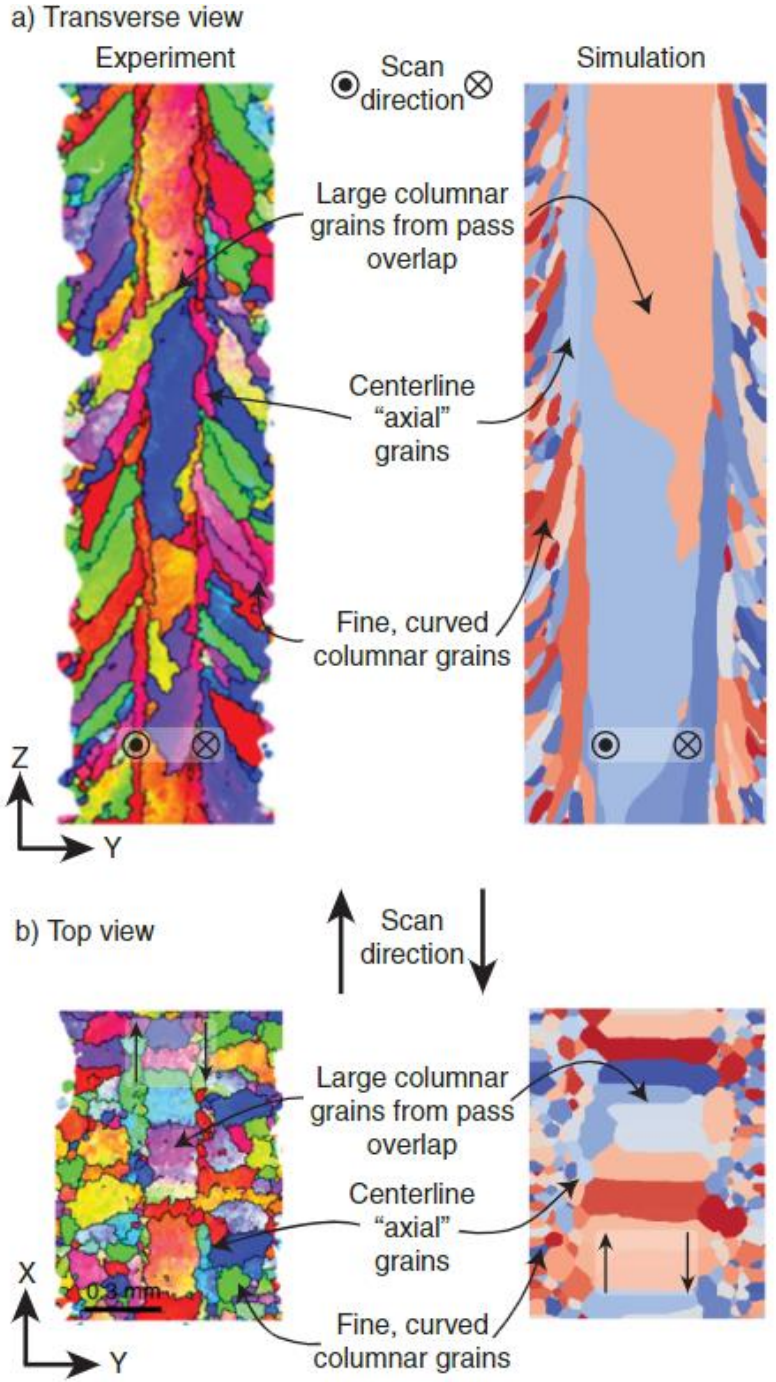

Fig. Comparison of AMed experimental and MC simulated microstructures on IN718 showing a good agreement

Source: Rodgers et al. 2017 [https://doi.org/10.1016/j.commatsci.2017.03.053]

Cellular automata equations

$$n(\Delta T) = \int_0^{\Delta T} \frac{dn}{d(\Delta T)}\, d\Delta T$$

$$\frac{dn}{d(\Delta T)} = \frac{n_{max}}{\sqrt{2\pi}} \exp\left[- \frac{(\Delta T - \Delta T_{mean})^2}{2\Delta T_\sigma} \right]$$

$$\Omega = \frac{C^* - C_0}{C^*(1-K)} = \mathrm{Iv}\left(\frac{\mathrm{VR}}{2\mathrm{D}}\right)$$

$$R = 2\pi \sqrt{\frac{\Gamma}{mG_c\xi_c - G}}$$

$$\xi_c = \frac{\pi^2}{K(\frac{VR}{2D})^2}$$

$$\Delta T = mC_0\left(1 - \frac{1}{\Omega(1-K)}\right)$$

ΔT: liquid undercooling

n: Continuous grain density

n_{max}: maximum nucleation density,

ΔT_{mean}: mean undercooling when nucleation occurs

ΔT_σ: standard deviation of the undercooling

Ω: solute supersaturation,

C*: liquid solute concentration at the dendrite tip,

C_0: initial solute concentration,

V: growth speed of the dendrite tip,

R: radius of the dendrite tip,

D:solute diffusion coefficient,

Iv :Ivantsov's solution,

K: partition coefficient,

m: liquidus slope,

Γ: Gibbs-Thomson coefficient, ξ_c

G_c: solute gradient,

G: temperature gradient,

ΔT: undercooling temperature

Summary

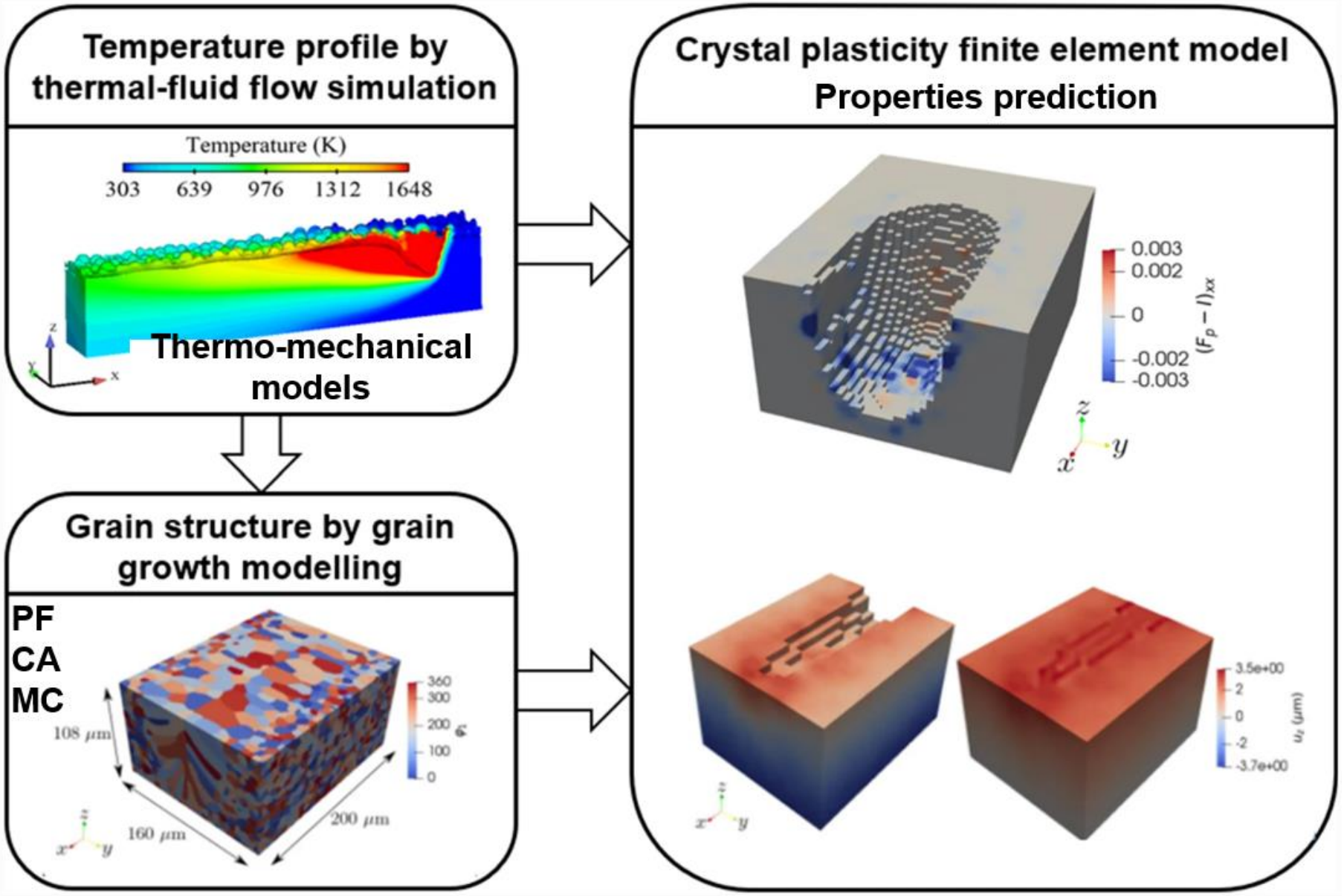

Fig. Integration of processing-microstructure-properties modelling in AM

Source: Grilli et al. 2022 [https://doi.org/10.1007/s00466-021-02116-z]